Quaternary Science Reviews 250 (2020) 106658

Contents lists available at ScienceDirect

Quaternary Science Reviews

journal homepage: www.elsevier.com/locate/quascirev

An end to the Last Interglacial highstand before 120 ka: Relative sea-level evidence from Infreschi Cave (Southern Italy)

Monica Bini [a, b, k, *], Giovanni Zanchetta [a, c, k], Russell N. Drysdale [d], Biagio Giaccio [c], Paolo Stocchi [f], Matteo Vacchi [a, k], John C. Hellstrom [g], Isabelle Couchoud [e], Lorenzo Monaco [h], Andrea Ratti [a], Fabio Martini [i], Lucia Sarti [j]

[a] Dipartimento di Scienze della Terra, University of Pisa, Italy
[b] Istituto Nazionale di Geofisica e Vulcanologia, Rome, Italy
[c] Istituto di Geologia Ambientale e Geoingegneria - CNR, Monterotondo, Rome, Italy
[d] School of Geography, The University of Melbourne, 3010, Victoria, Australia
[e] Laboratoire EDYTEM, UMR CNRS 5204, Universite' Savoie Mont Blanc, Universite' Grenoble Alpes, 73376, Le Bourget du Lac, France
[f] NIOZ - Royal Netherlands Institute for Sea Research, Coastal Systems (TX), And Utrecht University, P.O. Box 59, 1790, AB, Den Burg, Texel, the Netherlands
[g] School of Earth Sciences, The University of Melbourne, Melbourne, VIC 3010, Australia
[h] Dipartimento di Scienze Della Terra, Università La Sapienza di Roma, Rome, Italy
[i] Dipartimento di Storia, Archeologia, Geografia, Arte e Spettacolo, University of Florence, Prehistory Unit, Via S.Egidio 21, 50122, Firenze, Italy
[j] Dipartimento di Scienze storiche e dei Beni culturali, University of Siena, Via Roma 56, 53100, Siena, Italy
[k] CIRSEC - Centro Interdipartimentale di Ricerca per lo Studio degli Effetti del Cambiamento climatico dell'Università di Pisa

ARTICLE INFO

Article history:
Received 28 May 2020
Received in revised form
7 September 2020
Accepted 16 October 2020
Available online xxx

Keywords:
U/Th dating
MIS-5e
Highstand
Relative sea level
Last glacial inception
Solid earth geophysical models
Middle palaeolithic
Southern Italy

ABSTRACT

The timing, duration and evolution of sea level during the Marine Isotope Stage 5e (MIS 5e) highstand is a subject of intense debate. A major problem in resolving this debate is the difficulty of chronologically constraining the sea level fall that followed the peak of the highstand. This was mainly controlled by ice-sheet dynamics, the understanding of which is relevant for assessing future sea-level behavior due to global warming. Here we use stratigraphical and geochoronological (U/Th dating and tephra fingerprinting) evidence from the Infreschi archaeological cave (Marina di Camerota, Southern Italy) to constrain relative sea level (RSL) evolution during the MIS 5e highstand and younger stages. Uranium-thorium dating of speleothem deposition phases places the maximum highstand RSL at 8.90 ± 0.6 m a.s.l., as indicated by the near-horizontal upper limit of *Lithophaga* boreholes measured for along a ~3.5 km coastal cliff section. Geochronological data show that RSL fell more than 6 m before ~120 ka, suggesting a duration of the Last Interglacial highstand significantly shorter than proposed in some previous studies. Modelling shows that the RSL trend predicted by the ICE-5G and ICE-6G ice-sheet simulations is consistent with our data, but requires an additional significant reduction of both Greenland and Antarctic ice sheets to match the height of the local maximum highstand if no correction for tectonics is applied. Reconciling field data and models requires an earlier and likely shorter duration of the MIS 5e highstand. This suggests that our new data can constrain global ice-volume variations during the penultimate deglaciation, as well as glacial inception at the end of the Last Interglacial. According to our chronology, there is no local evidence of higher-than-present-day sea levels after 120 ka.

1. Introduction

Sea-level rise as a direct consequence of global warming is now well documented (e.g., Miller and Douglas, 2004; Clarke et al., 2016). Addressing outstanding questions and challenges regarding rates, magnitudes and sources of future sea-level rise requires integration of ice-sheet, sea-level and solid-Earth geophysical models supported by dense, globally distributed and well-dated relative sea-level (RSL) records (Dutton et al., 2015). The Last Interglacial (LIG), which occurred during Marine Isotope Stage 5e (MIS 5e), was a period of warmer temperature (e.g., 0.5–1.0 °C

* Corresponding author. Dipartimento di Scienze della Terra, University of Pisa, Italy.
E-mail address: monica.bini@unipi.it (M. Bini).

https://doi.org/10.1016/j.quascirev.2020.106658
0277-3791/

higher than pre-industrial values (Kaspar et al., 2005; Otto-Bliesner et al., 2013; Fischer et al., 2018). Due to this higher average global temperature, ocean thermal expansion (McKay et al., 2011) and massive ice melting produced a global sea-level at ~6 to ~8 m above the present one (e.g., Kopp et al., 2009; Dutton and Lambeck, 2012; O'Leary et al., 2013; Dutton et al., 2015), making the LIG a key period for evaluating current and future scenarios of sea-level rise. However, despite extensive investigations, conflicting interpretations on the different factors underlying the eustatic sea level during LIG persist. Uncertainties concerning the contributions of Greenland and Antarctica ice-sheet melting during the LIG (Dutton and Lambeck, 2012; O'Leary et al., 2013; Dutton et al., 2015; Rohling et al., 2019) result in different conclusions on the global sea level, presenting challenges for the correct understanding of the effects of future climate change. Similarly, the timing and rate of ice accumulation and related sea-level drop at the end of the LIG is also the subject of ongoing debate (e.g., Stirling et al., 1998; Moseley et al., 2013; Rohling et al., 2019).

The Mediterranean coast preserves a wide range of sedimentary and geomorphologic proxies related to the LIG highstand. These have been locally termed "Tyrrhenian" (Issel, 1914; see review in Asioli et al., 2005 and references therein). Previous work has identified at least two separate highstands (e.g. Bonifay and Mars, 1959), namely the "Eutyrrhenian" (assigned at ca. 125 ka, i.e. correlative to MIS 5e) and the "Neotyrrhenian" (assigned at ca. 100 ka or ca. 80 ka, that is, correlated to MIS 5a and MIS 5c). Although the recent accurate dating of Eutyrrhenian and Neotyrrhenian deposits on Mallorca has demonstrated they are both related to the MIS 5e highstand (Muhs et al., 2015), both earlier and more recent studies provide an inconsistent framework of the chronology and magnitude of MIS 5 sea-level oscillations. (i.e., Hearty et al., 1986; Mauz, 1999; Vesica et al., 2000; Jedoui et al., 2003; Zanchetta et al., 2004; Marra et al., 2019).

Two main sources of uncertainty in MIS 5 sea-level investigations in the Mediterranean lie at the heart of many of the current disagreements. The first concerns the integrity of the sea-level markers, which need to be collected with accurate elevation measurement and robustly related to contemporary mean sea level (e.g., the indicative meaning: Van De Plassche, 1986; Shennan et al., 2015). Strict adherence to these principles has not always been the case, especially in older studies, even if rigorous approaches have been followed in more recent work (Rovere et al., 2016). The second concerns the quality of the geochronological data, which has been obtained using different dating methods (e.g., thermoluminesce and/or optical-stimulated luminescence Mauz, 1999; amino-acid racemization, Hearty et al., 1986; U/Th, Vesica et al., 2000), each with its own degree of uncertainty and analytical limits. For example, many U/Th radiometric ages have been obtained on mollusk shells, in spite of the well-known issue of U mobility (e.g., Ivanovich et al., 1983; Hillaire-Marcel et al., 1996; Muhs et al., 2015).

For the Mediterranean region, there is scant radiometric data constraining the beginning of the RSL fall after the LIG highstand (Lorscheid et al., 2017; Ferranti et al., 2006). The availability of these data are vital for constraining the melting of Greenland and Antarctica ice sheets in response to global warming scenarios (Stocchi et al., 2018).

In this paper, we combine U/Th dating and tephrochronological data to constrain the timing of the RSL in a LIG sequence at Grotta di Infreschi (Marina di Camerota, Southern Italy, hereafter Infreschi Cave, Fig. 1) and compare these data with geophysical model RSL predictions. The data provide age limits on the phase of RSL decrease that followed the local MIS 5e highstand, and can shed new light on global ice-sheet dynamics immediately preceding and following the LIG.

2. Geological setting

Infreschi Cave (39°59′57″N, 15°25′33″E) is located on the Cilento Promontory, southern Italy, a large structural high between the Gulfs of Salerno and Policastro, ca. 4.5 km east of Marina di Camerota (Fig. 1). The cave is part of a larger, almost circular embayment (Baia d' Infreschi), and has formed in bedrock mainly composed of limestones and cherty limestones of the Mt. Bulgheria Mesozoic-Cainozoic units (Ascione et al., 1997). Limestone has been intensively karstified and several caves partly destroyed and/or modified by marine abrasion (Esposito et al., 2001).

Esposito et al. (2003) described the general stratigraphy of the cave. Sarti (1996) and Martini (2015) reported preliminary stratigraphic data on the continental infilling succession containing archaeological remains attributed to the Neanderthal presence in Middle Palaeolithic (research by L. Sarti in 1977–1985). Esposito et al. (2003) performed two U/Th ages (111.9 ± 11.0 and 91.7 ± 8.2 ka) on some flowstones using the alpha-counting method and interpreted the whole succession as substantially younger than MIS 5e, with the marine deposits correlated to the highstands of MIS 5a and 5c. The evidence of marine highstands are represented in the Baia di Infreschi by beach deposits and boreholes of the *Lithophaga lithophaga*, which show a clear horizontal-to-sub-horizontal upper limit.

From a geodynamic point of view, the area is dominated by extensional tectonics linked to counterclockwise rotation of the Italian peninsula related to the roll back of the lithospheric slab (e.g., Facenna et al., 2013). In terms of the elevation of MIS 5e deposits, Ferranti et al. (2006) consider the area to be relatively tectonically stable, with vertical movement estimates from ~0.03 mm/yr to ~0.07 mm/yr for the last ~125 kyr. The area is microtidal with maximal ranges of ca. ± 0.2 m (Naples Tidal Station; https://www.mareografico.it [accessed 29/01/2020]).

3. Material and methods

3.1. Fieldwork

Fieldwork was conducted between 2017 and 2018. Altitude measurements were obtained using a graduated rod equipped with a spirit level (repeated measurements on the same sea-level indicators yielded associated errors of $\leq \pm 0.1$ m; Zanchetta et al., 2014; Bini et al., 2018) and referenced to local biological mean sea-level indicators (Vacchi et al., 2020), which has often been used to determine the mean sea level with reasonable accuracy (±0.1 m) in microtidal Mediterranean settings (Laborel and Laborel-Deguen, 1996; Schembri et al., 2005; Vacchi et al., 2020). All elevations are expressed in metres above sea-level (m a.s.l.). The final elevation error associated with our measurements is ≤ 0.2 m. Fieldwork was focused on Infreschi Cave. However, in order to have a clearer and broader framework of the general tectonic behavior (i.e., homogenous vs variable uplift rate), we measured the elevation of the top of *Lithophaga* boreholes along the cliffs surrounding the Baia di Infreschi and near Marina di Camerota ca. 3.5 km apart (Fig. 1c). *Lithophaga* (date or boring mussels) live in the range of the upper limit of the infralittoral zone down to more than −30 m (Laborel and Laborel-Deguen, 1996). However, the highest concentrations are in the top few metres and their upper limit coincides closely with sea level (Pérès and Picard, 1964; Laborel and Laborel-Deguen, 1996; Rovere et al., 2015). Once clearly identified, the upper limit of the *Lithophaga* boreholes is considered a good indicator of past RSL (e.g. Ferranti et al., 2006; Rovere et al., 2016). Fig. 1 shows the position and elevation of the upper limit of the *Lithophaga* boreholes in the Baia di Infreschi and surroundings. Fig. 2 shows the

Fig. 1. Reference maps. **a)** and **b)** Location maps. Satellite imagery from Google Earth (imagery sources copyright 2014 Google and 2020 Maxar Technologies); **c)** sections where *Lithophaga* boreholes upper limit is identifiable. Lidar dada are from the Geoportale Nazionale http://www.pcn.minambiente.it/mattm/.

reconstructed stratigraphy of the cave integrated with the detail of the archaeological section (Sarti, 1996). The field survey, corroborated by new U/Th dating, allowed us to produce a new suite of sea-level data (e.g., index and limiting points) according to the protocol described by the International Geoscience Programme (IGCP) projects 61, 200, 495, 588, and 639 (e.g., Shennan et al., 2015; Padgett et al.., 2018; Khan et al., 2019).

3.2. U/Th dating

Samples for U/Th dating were selected in the field with the intention of chronologically constraining phases of speleothem concretions growth, which also infill boreholes following sea-level fall, using the lowest and outermost parts, and discarding concretions with obvious weathering. The selected blocks were extracted using a battery drill, cut and polished in the laboratory, then subsampled for dating using a dental drill at the Laboratory of Paleoclimatology and Geoarcheology, Department of Earth Sciences, University of Pisa. Samples were selected with the aid of thin sections to avoid potentially weathered samples and/or clastic-rich calcites. The U/Th dating was performed at the School of Earth Sciences, University of Melbourne, following the method described by Hellstrom (2003). Samples were dissolved and a mixed ^{236}U–^{233}U–^{229}Th spike was added prior to removal of the carbonate matrix with ion-exchange resin. A purified U and Th fraction diluted in nitric acid was introduced into a multicollector inductively coupled plasma mass spectrometer (MC-ICPMS Nu-Instruments Plasma). The $^{230}Th/^{238}U$ and $^{234}U/^{238}U$ activity ratios were calculated from the measured atomic ratios using a standardized parallel ion-counter procedure and calibrated against the HU-1 secular equilibrium standard. Correction for detrital contamination was applied following the method described by Hellstrom (2006) using an initial activity ratio of detrital thorium $(^{230}Th/^{232}Th)_i$ of 1.5 ± 1.5 (Table 1).

3.3. Tephra major element analyses

The major element composition of glass and pumice fragments from the tephra Inf-1 embedded in the inner part of the archaeological stratigraphic succession infilling the cave (Fig. 2) was measured to geochemically fingerprint the tephra and correlate it to a known and dated eruption. Analyses were performed using a wavelength-dispersive electron microprobe (WDS-EMPA) (Supplementary, Table S1) at the laboratory of the Istituto di Geologia Ambientale e Geoingegneria of the Italian National Research Council (IGAG-CNR) (Rome, Italy) using a Cameca SX50 electron microprobe equipped with a five-wavelength dispersive spectrometer. Operating conditions were set to 15 kV accelerating voltage, 15 nA beam current, 10–15 μm beam diameter, and 20 s per element counting time; Wollastonite (Si and Ca), corundum (Al), diopside (Mg), andradite (Fe), rutile (Ti), orthoclase (K), jadeite (Na), phlogopite (F), potassium chloride (Cl), barite (S), and metals

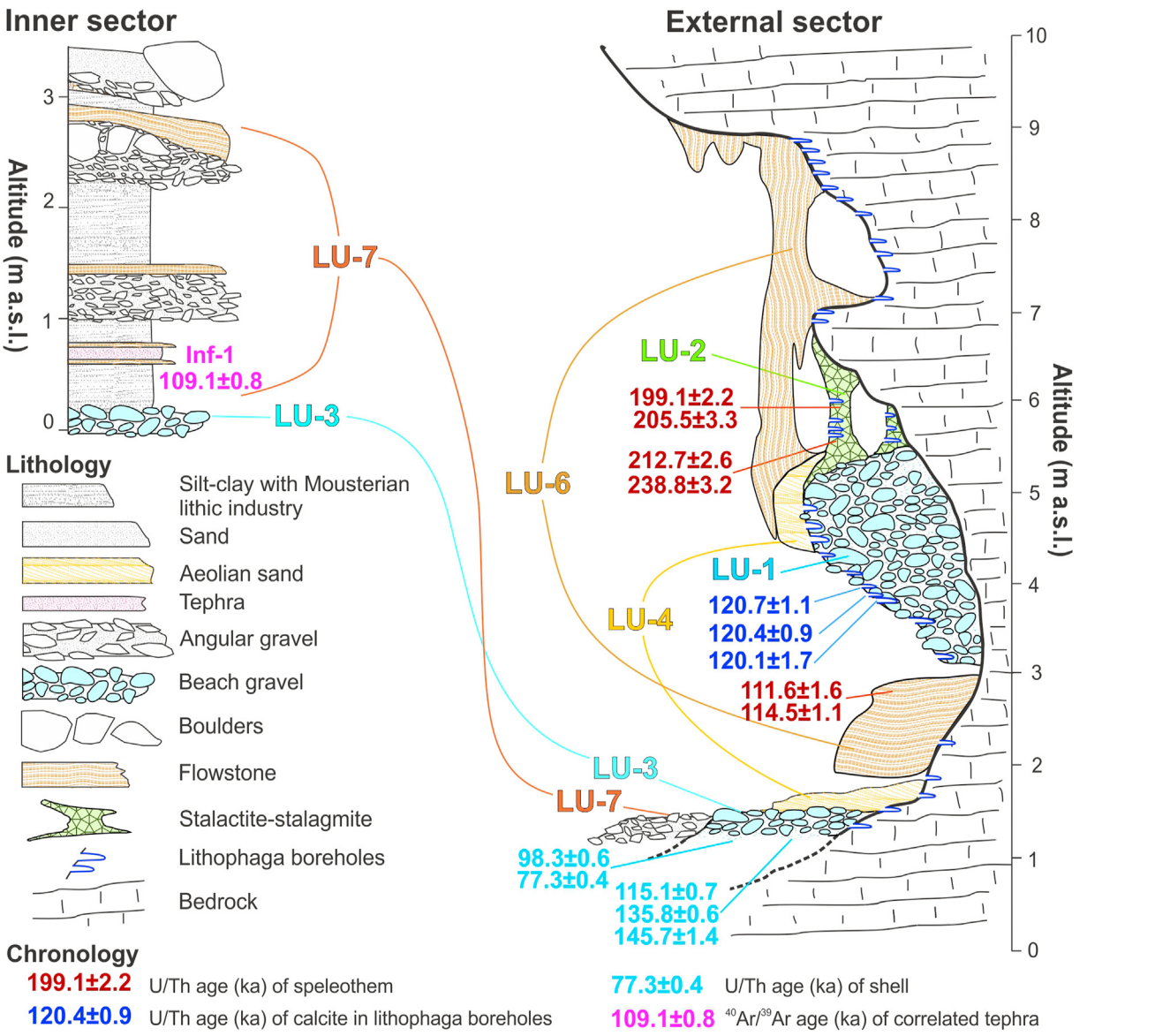

Fig. 2. Lithostratigraphic Units (LU) and geochronology of Infreschi Cave (modified after Esposito et al., 2003). The height scale is indicative to make it possible to view all the units.

Table 1
Corrected (in bold) and uncorrected U/Th (italic) ages. The activity ratios have been standardized to the HU-1 secular equilibrium standard, and ages calculated using decay constants of 9.195 $\times 10^{-6}$ (^{230}Th) and 2.835 $\times$ 10^{-6} (^{234}U). *Molluscs.

Lab. Sample ID	Field Sample ID (altitude m asl)	^{238}U (ng/g)	[^{230}Th/^{238}U]	[^{234}U/^{238}U]	*Age$_{unc}$ ka (95%)*	[^{232}Th/^{238}U]	[^{230}Th/^{232}Th]	Age$_{corr}$ (ka) (95%)	[^{234}U/^{238}U]$_i$
UMD180823-345	INF18/1A (4.12)	230	0.8939 (0.0023)	1.0318 (0.0016)	*214.20 (2.10)*	0.009439 (0.000072)	90.74	**212.74 (2.58)**	1.0579 (0.0027)
UMD180823-349	INF18/1B (4.12)	272	0.9327 (0.0028)	1.0390 (0.0017)	*239.50 (3.10)*	0.004745 (0.00032)	196.47	**196.47 (3.22)**	1.0765 (0.0032
UMD180823-340	INF18/3A (4.51)	237	0.8674 (0.0027)	1.0262 (0.0016)	*199.97 (2.07)*	0.005496 (0.000061)	157.8	**199.11 (2.25)**	1.0460 (0.0027)
UMD180823-344	INF18/3B (4.51)	272	0.8771 (0.043)	1.0266 (0.0016)	*206.19 (3.17)*	0.004279 (0.000035)	205.0	**205.53 (3.28)**	1.0475 (0.0027)
UMD180823-386	INF18/5A (2.86)	148	0.6721 (0.0025)	1.0366 (0.0023)	*112.94 (0.89)*	0.008260 (0.000050)	81.4	**111.65 (1.58)**	1.0502 (0.0031)
UMD180823-420	INF18/5B (2.86)	166	0.6774 (0.0031)	1.0341 (0.0016)	*115.06 (0.99)*	0.003402 (0.000021)	199.1	**114.53 (1.33)**	1.0471 (0.0022)
UMD180823-362	INF18/4 (3.71)	401	0.7068 (0.0033)	1.0478 (0.0018)	*120.84 (1.10)*	0.000950 (0.000006)	744.1	**120.67 (1.12)**	1.0672 (0.0025)
UME190501-284	INF18/4A (3.73)	354	0.7079 (0.0023)	1.0488 (0.0015)	*120.41 (0.96)*	0.00334 (0.000067)	212.3	**120.35 (0.93)**	1.0685 (0.0021)
UME190812-343	INF18/4B (3.76)	504	0.7065 (0.0033)	1.0454 (0.0020)	*120.15 (1.66)*	0.0007452 (0.00014)	93.7	**120.09 (1.66)**	1.0639 (0.0028)
UME190501-222	INF18/2G (1.70)*	887	0.74935 (0.00226)	1.1300 (0.0015)	*115.10 (0.68)*	0.0004187 (0.000008)	17895.3	**115.03 (0.68)**	1.1799 (0.0020)
UME190501-218	INF18/2E (1.70)*	1318	0.85291 (0.00148)	1.1687 (0.0013)	*135,78 (0.58)*	0.0001965 (0.000004)	43400.7	**135.72 (0.56)**	1.2475 (0.0017)
UME190812-328	INF18/2F (1.70)*	1300	0.88059 (0.00373)	1.1645 (0.0020)	*145.71 (1.38)*	0.0004981 (0.000010)	17680.2	**145.66 (1.38)**	1.2481 (0.0028)
UMD180831-271	INF18/2A (1.70)*	-	0.5539 (0.0018)	1.0819 (0.0016)	*77.343 (040)*	0.000054 (0.000001)	10350.8	**77.33 (0.41)**	1.1019 (0.0019)
UME191014-374	INF18/2 (1.70)*	680	0.63727 (0.00193)	1.0643 (0.0019)	*98.33 (0.58)*	0.000063 (0.000001)	10132.3	**98.27 (0.57)**	1.0848 (0.0025)

(Mn) were used as standards. The Ti content was corrected for the overlap of Ti–K α peaks. In order to evaluate the accuracy of the electron-microprobe analyses, two international secondary standards (Kakanui augite and rhyolite RLS132 glasses from the United States Geological Survey) were measured prior of each analytical run. Details of the test results are reported in the Supplementary Table 2.

3.4. Sea level and glacial- and hydro-isostatic adjustment modelling

We investigated the contribution of glacial and hydro-isostatic adjustment (GIA) by means of forward numerical modelling. The GIA processes that locally modulate RSL change in response to ice-sheet fluctuations are described by the so-called sea-level equation (SLE; Farrell and Clark, 1976; Mitrovica et al., 1994; Stocchi and Spada, 2007). We solve the gravitationally and rotationally self-consistent SLE by means of the pseudo-spectral approach (Milne and Mitrovica, 2003; Stocchi and Spada, 2007). We account for time-dependent ocean functions (i.e. variable coastlines in time) and geocentric motion (Degree one). Solid Earth is assumed to be spherically symmetric, deformable but not compressible and radially stratified (Spada et al., 2004), and all the parameters depend on the radius (1D rheological model) characterized by linear Maxwell viscoelastic rheology. A purely elastic lithosphere and Maxwell viscoelastic mantle is divided into four layers based on the VM2 discretization (Peltier, 2004).

We employed ICE-5G and ICE-6G ice-sheets models (Peltier, 2004; Peltier et al., 2015), which describe continental ice thickness variations from 123 ka to the present-day. In order to simulate the actual MIS 5e transgressive peak that is also affected by the GIA signal from Termination II melting, we duplicate and combine each chronology in series, thus covering two glacial-interglacial cycles (from 246 ka to present day). In doing so, we are forced to make the crude assumption that the MIS 6 glacial maximum was equal to the Last Glacial Maximum (LGM), but geological and modelling evidence suggest that this was not the case (Lambeck et al., 2006; Colleoni et al., 2016; Creveling et al., 2015; Dendy et al., 2017; Rohling et al., 2017).

4. Results

4.1. A revised Infreschi stratigraphy

The Infreschi succession represents the remnant of a partially collapsed cavern, and contains seven main litostratigraphic units (LU) developed on the local carbonate substratum (Figs. 2–4). The older unit is a cemented gravelly beach deposit in a sandy matrix with sparse fossils (LU-1, Figs. 2 and 4a), directly resting on the vertical wall of the cave and discontinuously outcropping in the E side of the cave. This unit is covered by flowstone on top of which some stalagmites have grown (LU-2, Figs. 2, 3 and 4d). The general draping shape of the flowstone and the morphology of LU-1 indicate that LU-1 experienced a first phase of erosion and dismantling followed by the flowstone draping. Both surfaces of LU-1 and LU-2 units are densely riddled with *Lithophaga* boreholes (Figs. 2, 3 and 4d,e). In both sides of the cave, the *Lithophaga* boreholes terminate in a straight horizontal front at ~8.70 m a.s.l. on the vertical cave walls (Fig. 3).

A second gravelly, poorly-to-well cemented beach deposit with a sandy matrix rests on the cliff (LU-3, Figs. 2 and 4b). LU-3 contains abundant remains of *Chama* sp. mollusks, and is overlain by well-

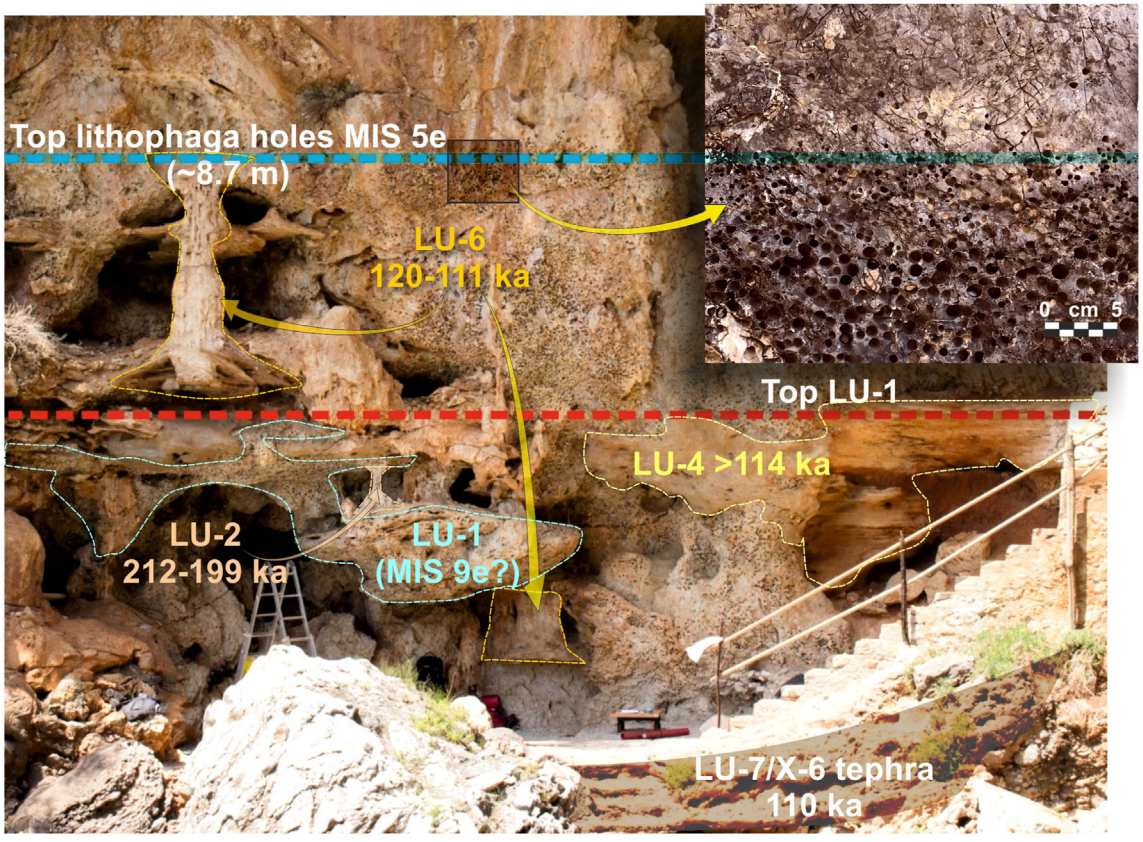

Fig. 3. General view of the western sector of the Infreschi Cave with the main morpho-stratigraphical features highlighted.

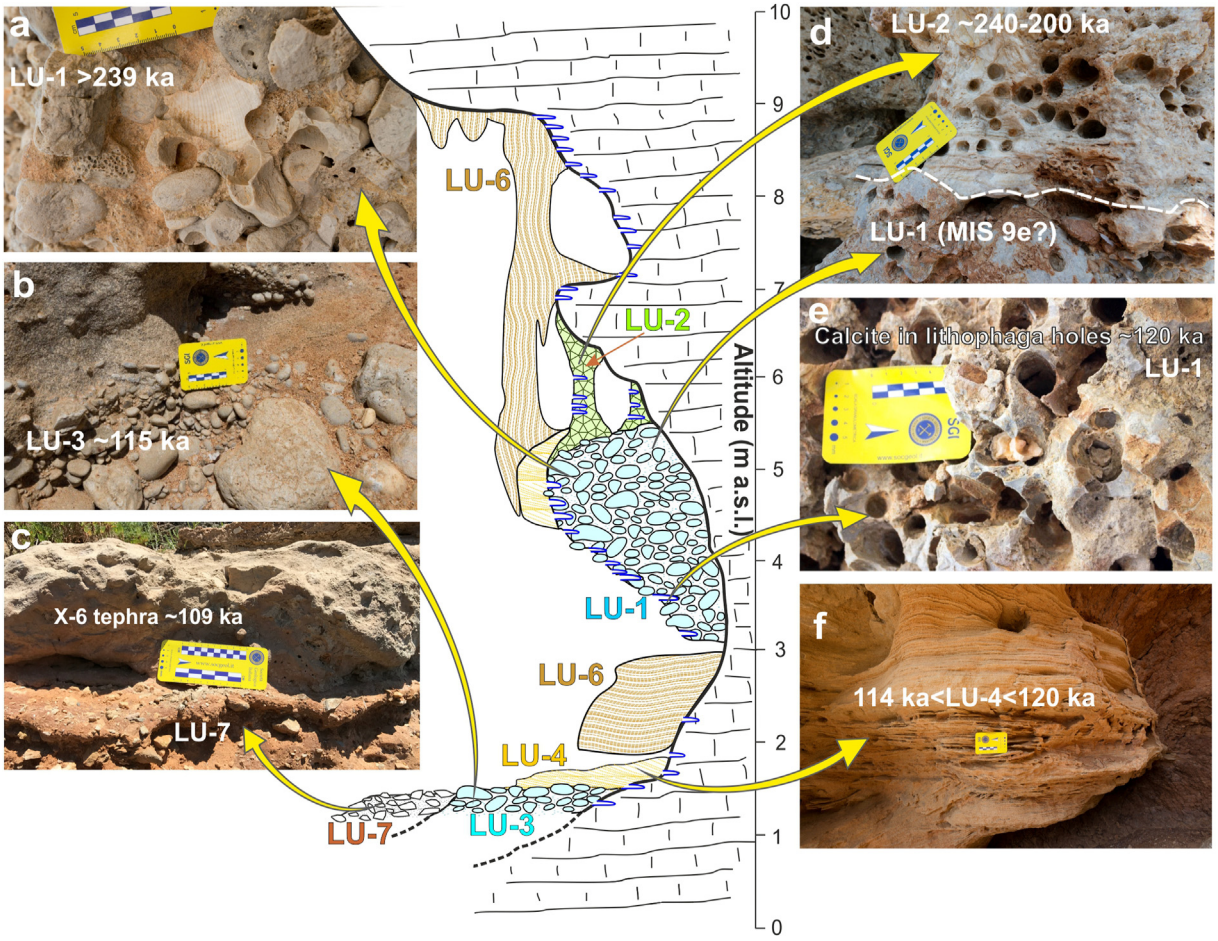

Fig. 4. Features of the main lithostratigraphic units (LU) recognized at Infreschi Cave. **a**: LU-1 beach deposits. Note the surface intersected by numerous *Lithophaga* boreholes; **b**: Beach deposits of the LU-3; **c**: view of the LU-7 archaeological deposit with the tephra layer correlated with the X-6 regional marker; **d**: contact between the LU-1 beach deposits and the first phase of speleothem deposition (LU-2). Note the surface of LU-2 with numerous *Lithophaga* boreholes; **e**: LU-1 with *Lihtophaga* boreholes with infilling of speleothem calcite; **f**: Aeolian sands (LU-4) with typical cross-stratification.

stratified and well-sorted medium sands of aeolian origin (LU-4, Figs. 2, 3 and 4f). Both LU-3 and LU-4 have buried the *Lithophaga* boreholes, indicating they are younger than the boreholes (Fig. 3). This succession is capped by a red paleosol (LU-5) containing ~50–60 cm of a reworked white volcanic ash layer (sample Inf-0) showing centimetric alternation of fine to coarse ash. The succession has been partially eroded and dismantled, and is capped by a phase of flowstone deposition (LU-6, Figs. 2 and 3) that forms a complex succession of draperies over the wall surface covering almost all previous LUs. The succession described thus far was completely carved and then filled by a succession of continental deposits (LU-7, see Figs. 2, 3 and 4e), resting on LU-3 and cover blocks containing *Lithophaga* boreholes and the cave walls. These deposits comprise a complex succession of blocks, breccias with a reddish matrix, and sandy-to-silty deposits, containing Middle Paleolithic artifacts and bone remains ("Musterian", Sarti, 1996; Martini, 2015, Figs. 2 and 4c). Importantly, the lower part of this continental clastic succession contains a decimetric-thick and massive tephra layer (Inf-1, Figs. 2 and 4c). Large blocks and boulders probably representing the final collapse of the cave structure seal the whole succession.

In Infreschi Cave, and in the greater part of the Baia di Infreschi and the area of Marina di Camerota, there is a very clear evidence of the upper limit of the *Lithophaga* boreholes. The mean altitudinal values of the upper limit measured in four sections where it can be followed reasonably well over a distance of ca. 3.5 km, is 8.7 ± 0.6 m a.s.l. (Figs. 1 and 3).

4.2. Uranium–Thorium chronology

The top and the very base of the LU-2 flowstone-stalagmite system were dated using U/Th, returning an age range of ~240-200 ka (Fig. 2 and Table 1). The age reported by Esposito et al. (2003) for this unit was ~111 ka. Three samples from different speleothem calcite *Lithophaga* borehole fillings, representing the early stages of the LU-6 concretion phase (Fig. 2; 4e) and collected at ca. 3.70 m a.s.l., yielded consistent ages of ~121-120 ka (Fig. 2 and Table 1). This is in agreement with the outer samples of the LU-6 flowstone collected at 2.86 m a.s.l., which yielded two ages of ~115 and ~112 ka. This latter unit was dated by Esposito et al. (2003) at ca. 90 ka. This is more consistent with our data, as Esposito et al. (2003) may have sampled a younger portion of this flowstone deposition phase. Considering the consistency of our U/Th dating for LU-2, and the good agreement with Esposito et al. (2003) for LU-6, we believe that, rather than a problem of dating (MC-ICPMS can have 20–40 better accuracy than alpha dating, e.g., Hellstrom, 2006), the marked difference in the dating results for LU-2 (i.e., ~240–200 ka vs ~111 ka) suggests a sampling problem, which, due to the complex

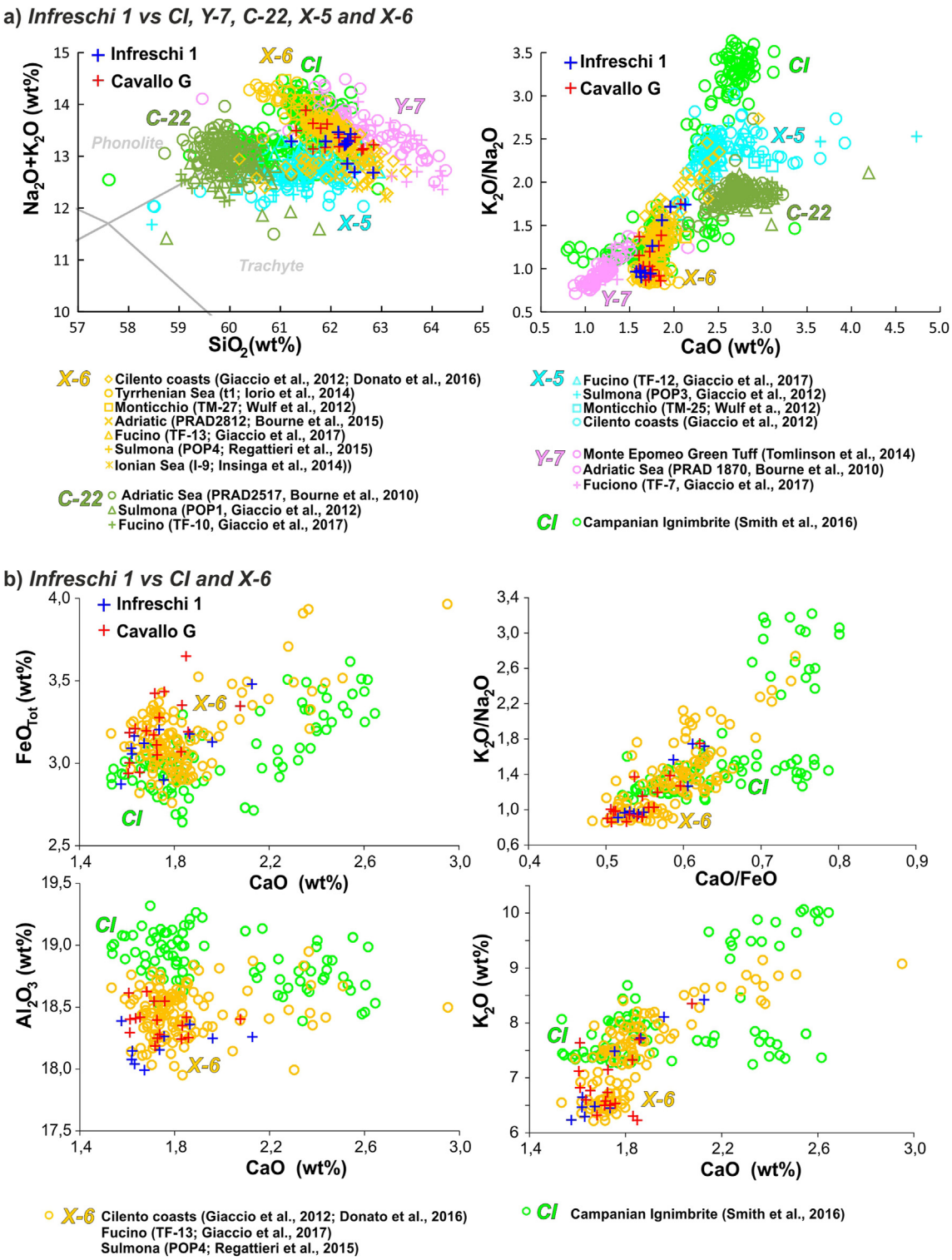

Fig. 5. Representative major elements composition for the tephra layer Inf-1 from LU-7 of the Infreschi succession and the equivalent tephras. **a**) Total alkali versus silica classification diagram (left; Le Bas et al., 1986) and CaO/FeO vs Cl source-discriminating diagram (right; Giaccio et al., 2019) for the layer Inf-1 and for the major Campi Flegrei tephra markers spanning the 115–40 ka interval. **b**) Selected bi-blots for the Inf-1, Campanian Ignimbrite and X-6 tephra, showing that the best geochemical matching is with the X-6 tephra (data source are reported in legend). For comparison, the composition of Layer G of Grotta del Cavallo, correlated to the X-6 tephra (Zanchetta et al., 2018), is also shown.

draping of the different generations of flowstone-stalagmite, can locally be overlapped by the younger LU-6.

Finally, series of subsamples from two different individuals of *Chama* sp. shells collected from the LU-3 beach deposits yielded inconsistent ages between ~77 and 145 ka (Fig. 2).

4.3. Tephra glass composition

The tephra layer Inf-0 within LU-5 is highly altered and, although sampled at different points, yielded no suitable samples for chemical analyses.

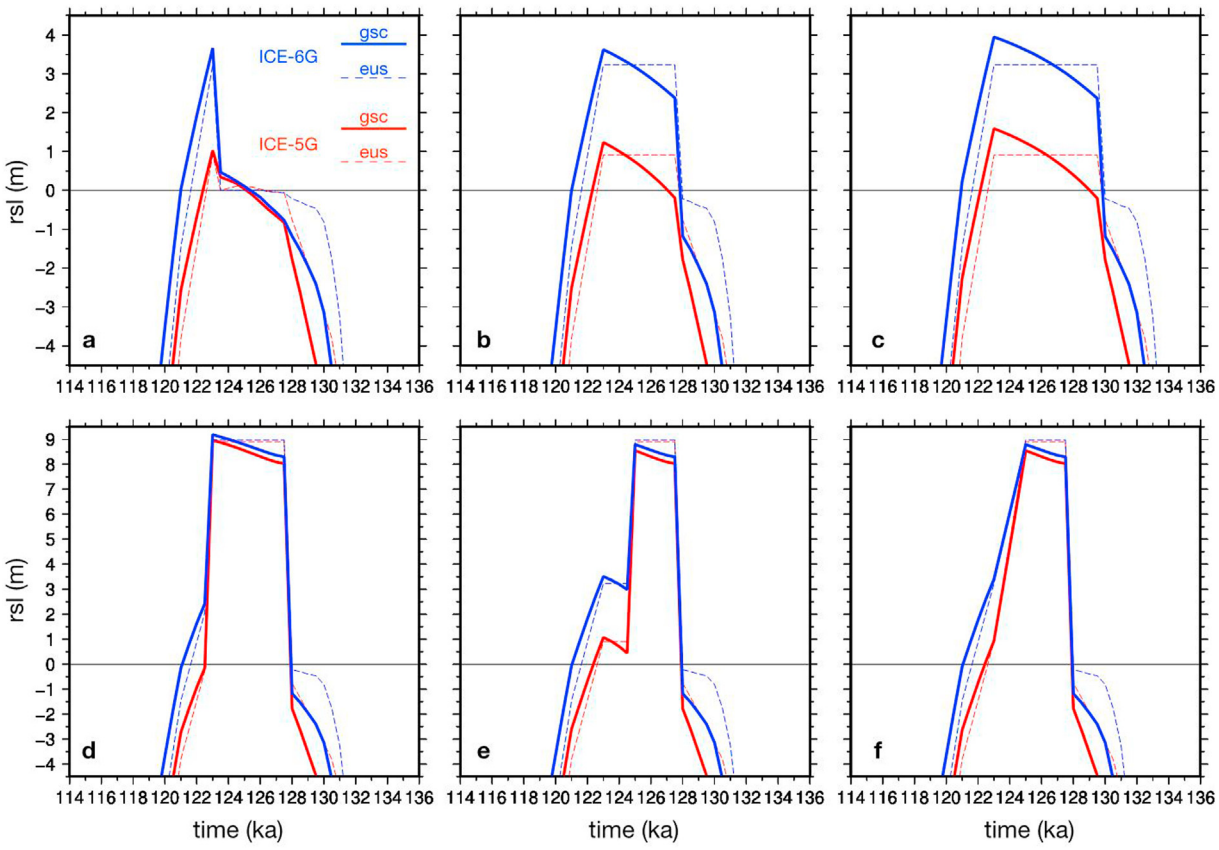

Fig. 6. Predicted RSL curves according to ICE-5G and ICE-6G ice sheets models and VM2 mantle viscosity profile. The solid curves represent the gravitationally self-consistent GIA process while the dashed curves show the eustatic trend. *a*, standard ice-sheet chronologies combined in series. *b*, extended highstand. *c*, extended highstand with a further 2000-year extension. *d*, scaled GrIS and AIS melting with a total of 9 m eustatic rise. *e*, same as *d* but with a step-wise eustatic drop at 125 ka. *f*, same as *e* but with linear eustatic drop.

Glass shards from the Inf-1 tephra embedded in LU-7, within the archaeological succession, instead show good preservation, and are well-suited for EMPA-WDS analyses. The volcanic glass has an almost homogenous trachytic composition (Fig. 5a, left), featuring a SiO_2 content ranging between ~62.8 wt % and 61.2 wt % and by a relatively narrow variability of the K_2O/Na_2O ratio (~1.7–0.9). As a whole, the composition of this layer shows the typical features of Campanian tephras (e.g., Tomlinson et al., 2012, 2015). In particular, according to the CaO/FeO vs Cl discriminating diagram (Giaccio et al., 2017, 2019), it can be ascribed to Campi Flegrei, with which it shares a similar high content of Cl (~0.5–1.0 wt%) and relatively low CaO/FeO (~0.5–0.6).

4.4. Numerical models

The gravitationally self-consistent GIA modelling shows that the area is affected by subsidence. Here, the dominant signal is the water-loading term, which causes a generalized subsidence of the centre of the Mediterranean Sea (Lambeck and Purcell, 2004; Stocchi and Spada, 2007; Stocchi et al., 2018). The viscous response of the Earth's mantle drives a monotonous RSL rise (solid curves in Fig. 6a) that delays the crossing of present-day mean sea level with respect to eustatic sea level (dashed curves in Fig. 6a). Both ice-sheet chronologies show that the eustatic sea level is very close to the present-day at 127.5 ka. However, the GIA keeps the local RSL ~1 m lower than today at 127.5 ka, and then drives a monotonous ~1.5 m rise until 123.5 ka for both models. Interestingly, this shows that the difference in MIS 6 glacial configuration between ICE-5G and ICE-6G can no longer be appreciated in this area, and the GIA signal is purely dominated by the Earth's mantle rheology.

The sudden eustatic jump at 123 ka that characterizes both models is an artefact of the repetition in time of two consecutive chronologies. ICE-5G is characterized by a ~1 m rise mostly driven by Greenland Ice Sheet (GrIS) melting, while ICE-6G is characterized by ~ 3.5 m rise stemming from both GrIS and Antarctic Ice Sheet (AIS) melting. A sudden RSL drop follows the highstand in both models and the crossing of the present-day mean sea level is again delayed with respect to the eustatic (dashed curves) by the viscous response of the mantle.

We further modify the two ice-sheet chronologies by extending the highstand peak between 123 and 127.5 ka through the scaling of GrIS and AIS thickness (Fig. 6b). The results show that an extended highstand period results in a ~0.5 m higher peak at 123 ka in response to the GIA-induced subsidence The deviation of the local GIA-modulated RSL curve from the eustatic curve further increases when 2000 years of static ice-sheets volume are added to the chronology (Fig. 6c). Accordingly, the longer relaxation time allows the local GIA response to drive a higher maximum highstand peak. Of course, this pattern strongly depends on the mantle viscosity profile as well as other rheological parameters that describe the solid-Earth model (Stocchi et al., 2018).

Considering the Infreschi RSL morpho-stratigraphic data, and especially the elevation of the *Lithophaga* boreholes at ca. 9 m a.s.l. (see sections 4.1. and 4.2), we also performed a second run by scaling the GrIS and AIS thickness to approach the elevation of the observed RSL biomarkers (Fig. 6d). The predicted GIA trend remains the same, but the maximum highstand is now higher (Fig. 6d). We applied a further modification by including a two-step highstand in

both ice-sheet chronologies: the maximum eustatic highstand is maintained until 125 ka and is then lowered to the original value at 124.5 ka (Fig. 6e). Accordingly, the GIA results in a small RSL rise (secondary fluctuation) between 124.5 and 123 ka (Fig. 6e). Finally, we also allow for a linear ice thickness increase between 125 and 120 ka, which results in a monotonous RSL drop (Fig. 6f).

5. Discussion

5.1. Tephra correlation

Considering the U/Th chronology and archaeological constraints, the tephra Inf-1 in LU-7 should be younger than ~115 ka and likely older than ~40 ka (late Marine Isotope Stage 3, MIS 3), which is the uppermost limit of the Mousterian (Higham et al., 2014). The tephra could thus be associated with a number of Campi Flegrei, or Campi Flegrei-like, tephras known from the 115–40 ka interval, among which the Campanian Ignimbrite (CI), C-22, X-5 and X-6 are the most widespread (e.g., Bourne et al., 2010; 2015; Wulf et al., 2012; Giaccio et al., 2012; 2017; 2019; Insinga et al., 2014; Sulpizio et al., 2010; Tomlinson et al., 2015; Leicher et al., 2016).

The total-alkali-versus-silica classification diagram allows exclusion of many of these tephra layers, keeping as potential correlatives only the CI and X-6 tephras (Fig. 5a, left). However, although the glass composition of the CI and X-6 appear quite similar, using some selected oxides, such as Al_2O_3, K_2O, FeO_{tot}, which allow us to readily discriminate CI from X-6, the composition of Infreschi 1 tephra matches very well that of X-6 (Fig. 5b). The X-6 tephra is an important and widespread tephra that in Mediterranean marks the first pronounced stadial of MIS 5, corresponding to Greenland Stadial GS24 or the North Atlantic cold event C23 (e.g., Sulmona Basin: Regattieri et al., 2015; Fucino Basin: Mannella et al., 2019; Lake Ohrid: Zanchetta et al., 2016; Tenaghi Philippon: Wulf et al., 2018). Its best current radiometric dating has been determined by the $^{40}Ar/^{39}Ar$ method of sanidine extracted from the Sulmona and Tyrrhenian Sea X-6 tephra, which yielded the ages of 109.1 ± 0.8 ka and 108.9 ± 1.8 ka, respectively (Regattieri et al., 2015; Iorio et al., 2014). This tephra has also been found within "Musterian" layers at Grotta del Cavallo in southern Italy (Zanchetta et al., 2018), confirming the importance of this tephra in constraining the age of the Middle Palaeolithic of the Central Mediterranean.

5.2. Palaeoenvironmental reconstruction

The results of the stratigraphical-geomorphological investigations indicate that the cave experienced two marine transgressions and regressions, documented by the shallow marine lithofacies of LU-1 and LU-3 and by the transitional-to-continental lithofacies of LU-2, LU-4, LU-5, LU-6 and LU-7, respectively (Fig. 2). Overall, this paleoenvironmental framework is similar to that proposed by Esposito et al. (2003), but the more detailed morpho-stratigraphical and geochronological data acquired in this study allow us to better and precisely constrain the succession of depositional-erosional events, which are summarized in the following paragraphs.

The first evidence of marine deposits is LU-1 (Figs. 2 and 4a), which is covered by the first phase of concretions of LU-2 dated to MIS 7 (Fig. 2); consequently, LU-1 can be attributed to a previous highstand, i.e., MIS 9e interglacial or earlier (Fig. 7; e.g., Lisiecki and Raymo, 2005; Railsback et al., 2015).

After a long phase of emergence, during which the MIS 7 flowstone LU-2 formed (Fig. 7), Infreschi Cave experienced a second marine transgression, which was responsible for the formation of the *Lithophaga* boreholes up to an elevation of ~8.7 m and the deposition of the beach deposits of LU-3 (Figs. 2, 3 and 4b). Because both LU-1 and LU-2 are extensively burrowed by *Lithophaga*, the ages of the LU-2 flowstone/stalagmites also constrain the chronology of this second marine ingression, which has to be younger than MIS 7. The upper chronological limit of this marine emergence is precisely constrained by age of the morpho-stratigraphic markers of the subsequent marine regression, represented by the speleothem deposition phase, which covers and/or fills the *Lithophaga*

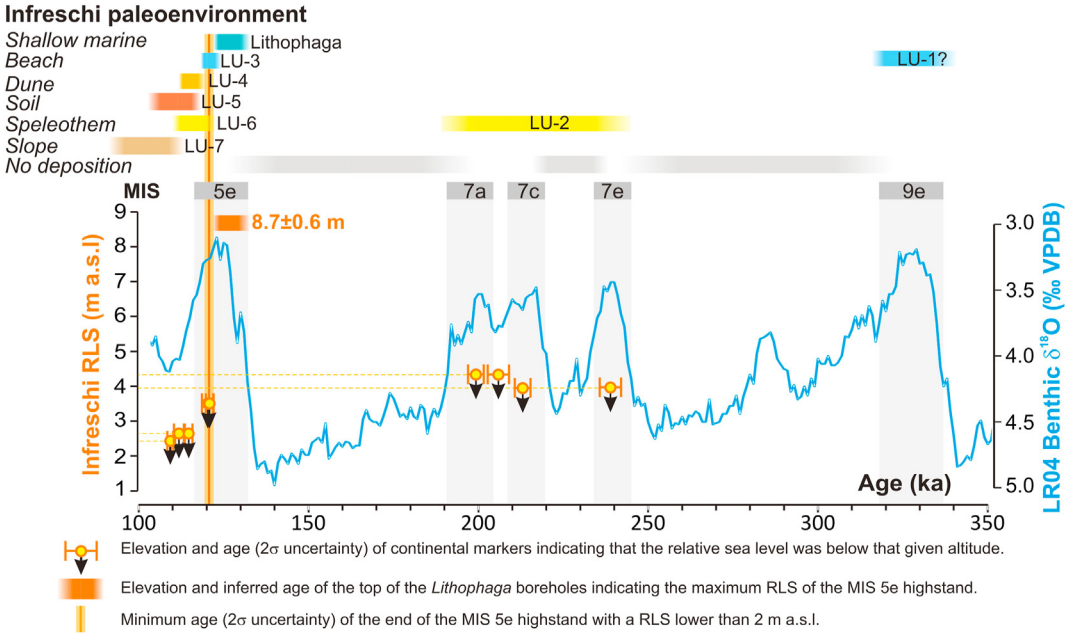

Fig. 7. Chronology of the main stages of the paleoenvironmental evolution and Relative Sea Level (RSL) of the Infreschi Cave plotted against the benthic stack record from Lisiecki and Raymo (2005).

boreholes, and by the continental deposits containing the X-6 marker tephra (LU-6 and LU-7, Fig. 2). The U/Th dating of LU-6, including the calcite that infills the *Lithophaga* boreholes (Fig. 2 4f), between ~120 and ~111 ka, and the X-6 tephra of ~109 ka, precisely constrain the age of the *Lithophaga* boreholes to the maximum highstand of MIS 5e (Fig. 7).

As far as the age of the shells in the beach deposits of LU-3 is concerned, the scattered results between ~77 and ~145 ka merely confirm the general unreliability of the age of these samples because of the high mobility of U in shells (e.g., Muhs et al., 2015). This is supported by the U content, which is higher than expected for marine shells (e.g., >0.6 ppm, Ivanovich et al., 1983; Aliyev and Sari, 2003), indicating post-mortem U uptake. However, the $^{234}U/^{238}U_{initial}$ activity ratio is close to (1.17 ± 0.08), that expected for marine carbonates (i.e., ~1.15; e.g. Hibbert et al., 2016; Medina-Elizalde 2013). Whilst it is not decisive to assign a firm age for LU-3, the position of the shells with respect to the LU-6 flowstone, which developed above LU-3, links LU-3 to a late stage of the MIS 5e highstand, postdating the phase of *Lithophaga* bioerosion that occurred prior to 120 ka (Fig. 7).

Finally, the development of the dune deposits of LU-4, which overlie the LU-3 beach deposits (Fig. 2), indicates a further marine regression. Although no direct chronological indication is available for this later stage of the sea level fall, it has to be younger than LU-3, and older than the overlying LU-7, which contains the X-6 tephra dated to ~109 ka (Fig. 2). This marks the definitive, full post-LIG emergence of Infreschi Cave (Fig. 7).

5.3. Implications for the relative sea level during MIS 9(?)-MIS 5 highstands

The new dataset allows the production of a new suite of RSL index and terrestrial limiting points (Table 2), which provides fresh insights into sea-level positions for the last ~240 ka.

MIS 9e and MIS 7 – Our data cannot provide detailed information for the relative sea level (RSL) during the MIS 9 (or an older interglacial) and MIS 7 highstands; only qualitative conclusions can be made. Specifically, considering, on one hand, the elevation of the LU-1 beach deposits, possibly representing the MIS 9e, and the absence of any marine evidence attributable to MIS 7, on the other, we can just conclude that RSL during MIS 9e should have been >6 m a.s.l. (Figs. 3 and 5), while during MIS 7 it was likely below present sea level. This is consistent with the data on a submerged stalagmite from Argentarola Cave in central Italy (e.g. Bard et al., 2002).

MIS 5e – As described in section 4.2, *Lithophaga* boreholes show a consistent pattern over a large area with a well identified, sub-horizontal upper limit in particular in the Infreschi area. This indicates that the investigated sectors of the coast have experienced minimal differential tectonic uplift. Therefore, the upper limit should closely represent the Mean Lower Low Water (mllw) level that, in the Mediterranean (and specifically in the area), is ca. 20–25 cm below Mean Sea Level (MSL, Laborel and Laborel-Deguen, 1996), assuming a tidal range comparable to today. Therefore, the horizontal line of the upper front of the Lithophaga boreholes can be considered a close approximation for the RSL in the area during MIS 5e highstand. Once corrected for the tidal excursion of ~20 cm, this gives 8.90 ± 0.6 m a.s.l. (Fig. 3). An additional marker for RSL would be represented by the transition between the gravel beach deposits of LU-3 and the aeolian sand of the LU-4, which represents a terrestrial limiting point (i.e., a point that constrains the RSL below a given elevation, Rovere et al., 2016). Even though this limit is not chronologically well constrained, its age should be younger than the highstand indicated by the *Lithophaga* boreholes, but older than the U/Th of speleothems, indicating the RSL was lower than or close to ~2 m a.s.l. before 120 ka (Fig. 7). Speleothems can also be considered terrestrial limiting points (Table 2) because their formation is not possible below sea level. For this reason, the U/Th dating of the calcite speleothem filling the *Lithophaga* boreholes is of particular interest to constrain the RSL drop after the highstand peak. Three independent but internally consistent U/Th ages indicate deposition of speleothem calcite at ~120 ka. This should represent the oldest phase of LU-6 flowstone, implying that by ~120 ka at least ~6 m of sea level lowering occurred from the highstand peak at 8.70 m a.s.l. (Fig. 7). The top of the lower flowstone drape (LU-6, Fig. 2) indicates no RSL rise occurred between 120 and 11 ka. This is further confirmed by the ~109 ka age of the tephra layer within the lower portion of LU-7 containing the Paleolithic artifacts. The Infreschi Cave record cannot tell us about the timing of the highstand, but ultimately it indicates that RSL was already below at least 2 m a.s.l. before 120 ka.

According to the model outputs shows in Fig. 6, the initial differences between the inferred and predicted RSL fluctuations, either in the maximum vertical elevation or in the timing and length of the RSL highstand, can be reduced by modifying the ice-sheet chronologies, assuming no tectonic displacement of our markers to higher or lower elevations.

In particular, the predicted RSL curves according to ICE-5G and ICE-6G, although being characterized by lower highstands (between 2 and 4.5 m), reach the present-day sea-level elevation before 120 ka; i.e. consistent with the observed drop of at least ~6 m between 125 and 120 ka (Fig. 6a–c). However, because the viscous response of the Earth's mantle tends to delay the occurrence of the transgressive peak and to reduce or increase its maximum elevation (with respect to the eustatic value) according to the duration (time window), a ~6m RSL drop commencing by 125 ka implies that the volumetric reduction of Greenland and Antarctic ice sheets was significant, early and occurred relatively rapidly. This is, for instance, in agreement with model simulations of AIS contribution to global mean sea level performed by De Conto and Pollard (2016), which show an early important contribution from the AIS, which progressively decrease after ~125 ka. This is consistent also with

Table 2
New suite of RSL index points (IP) and terrestrial limiting points (TLP) produced in this study. IR is the indicative range. Elevations are expressed in m above the modern mean sea level.

Dated facies	Age (kyr)	Elevation (m)	IR	RSL (m)	Type
Upper limit of *lithophaga* holes	5e	8,7 ± 0,6	mllw-msl	8.9 ± 0,6	IP
Speleothem	199,1 ± 2,2	4,5 ± 0,1	above msl	<4,51 ± 0,1	TLP
Speleothem	205,5 ± 3,3	4,5 ± 0,1	above msl	<4,51 ± 0,1	TLP
Speleothem	212,7 ± 2,6	4,1 ± 0,1	above msl	<4,12 ± 0,1	TLP
Speleothem	238,8 ± 3,2	4,1 ± 0,1	above msl	<4,12 ± 0,1	TLP
Calcite in lithophaga holes	120,7 ± 1,1	3,7 ± 0,1	above msl	<3,71 ± 0,1	TLP
Calcite in lithophaga holes	120,4 ± 0,9	3,7 ± 0,1	above msl	<3,73 ± 0,1	TLP
Calcite in lithophaga holes	120,1 ± 1,7	3,8 ± 0,1	above msl	<3,76 ± 0,1	TLP
Tephra in Aeolian sand	109,1 ± 0,8	2,7 ± 0,1	above msl	<2,7 ± 0,1	TLP

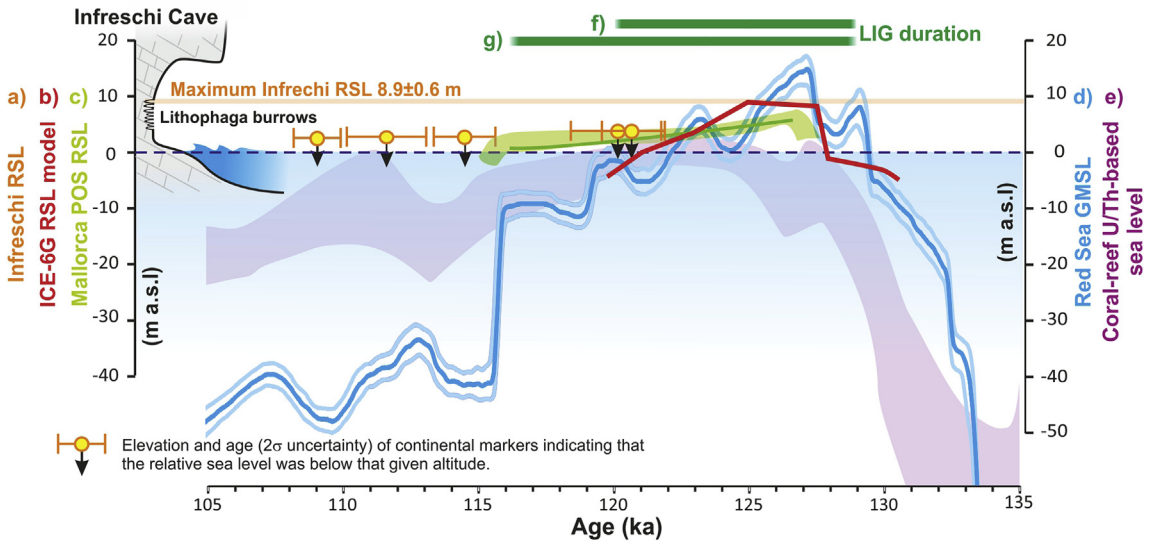

Fig. 8. Relative Sea Level (RSL) data from Infreschi Cave compared with both global and Mediterranean reference records. **a)** Infreschi Cave RSL record including the elevation and the age (±2s uncertainty) of the continental markers indicating that the RSL was below that given altitude. **b)** Output of the ICE-6 model of Fig. 6g **c)** Mediterranean RSL from Mallorca Island, based on phreatic overgrowth stalagmite (POS) corrected for GIA (Polyak et al., 2018). **d)** Global Mean Sea Level (GMSL) approximation based from Red Sea core KL11 PM (dark blue line) and its 95% probability interval (pale blue lines) (modified after Rohling et al., 2019). **e)** Monte Carlo 95% confidence interval of selected U/Th dating ($\delta^{234}U_i$ 137–157‰) of sea level markers from global coral reefs (Medina-Elizalde, 2013). **f)** and **g)** Duration of the Last Interglacial (LIG) highstand based on U/Th chronology of Bahamas (Chen et al., 1991) and Australia (Stirling et al., 1998) coral reefs, respectively. (For interpretation of the references to colour in this figure legend, the reader is referred to the Web version of this article.)

data presented by Rohling et al. (2019), which indicate an AIS derived highstand from ~129.5 to 125 ka. A significant contribution of AIS melting was also proposed for the early stage of the T-II deglaciation, i.e., during the meltwater pulse event associated with Heinrich stadial 11 (~135–130 ka), which through a bipolar seesaw mechanism likely resulted in a sustained Antarctica warming (Marino et al., 2015). We also propose that an earlier and shorter highstand event, as suggested by the new data, points to a rapid retreat of the North American and Eurasian MIS 6 ice-sheets during Termination II.

The differences in the local measured RSL highstand indicated by *Lithophaga* boreholes and for instance ICE-5G and ICE-6G model of Fig. 6a–c may depend on several assumptions in the model and inaccuracy in the input parameters. We can also presume that part of the difference is related to a small tectonic uplift of the area and thus the geophysical model could be used to estimate the values (Creveling et al., 2015). Considering the altitudinal differences between the highstand in the ICE-5G and ICE-6G models (Fig. 6a–c) and the top of the *Lithophaga* boreholes, we obtain a maximum range of the uplift rates from ca. 0.05 to 0.04 mm/yr, which can be considered a further refinement of the previous regional data indicated by Ferranti et al. (2006). However, the calculated values again suggest relatively minor tectonic uplift in this area in the last thousands of years, as supported also by detailed local studies based on other geological evidence on the position of the Lower Pleistocene and Pliocene shorelines (Ascione and Romano, 1999). In any case the eventual presence of these tectonic movements does not affect the general finding from the Infreschi Cave and the chronology of the RSL. The model outputs of Fig. 6d–f assume lower long-term tectonic component. However, the different scenarios do not conflict with the point of rapid RLS drop before 120 ka.

Comparing our RSL values with regional or global data obtained, for instance, on coral dating from "far field" sites (e.g., Chen et al., 1991; Stirling et al., 1998; Medina-Elizalde, 2013), and the modelled Red Sea stack of Rohling et al. (2019) is challenging for the different GIA correction and potential tectonic biases, which can exist between sites. With this in mind, Fig. 8 shows the Infreschi data and the ICE-6G output model plotted along with Red Sea and other Mediterranean and global reference records of mean seal level. The Infreschi data are in good agreement with modelled Red Sea global stack (Rohling et al., 2019, and references therein), placing the end of the LIG sea-level highstand sometime before 120 ka, when RSL at Infreschi had already dropped by 6 m. Our data is also consistent with speleothem growth in a now submerged cave in the Yucatan, indicating that at ~118 ka local RSL was already significantly below present sea level (Moseley et al., 2013). Therefore, although being indicators of the local RSL variation, the new data provide further constraints to global ice-sheet volumetric reconstructions (Waelbroeck et al., 2002; Siddall et al., 2003; Grant et al., 2014).

On the other hand, our new data are in disagreement with other scenarios characterized by a late MIS 5e highstand. In particular, O'Leary et al. (2013), using stratigraphic and geomorphic mapping and uranium-series geochronology of fossil coral reefs and geophysical modelling of sea-level records from Western Australia, concluded that eustatic sea level rose to about 9 m above present at the end of the LIG (between ca. 120 and 118 ka), suggesting that in the last few thousand years of the interglacial, a critical ice-sheet stability threshold was crossed, resulting in the catastrophic collapse of polar ice sheets and substantial sea-level rise. This seems to have occurred while RSL at Infreschi decreased. Moreover, data from U/Th dating of phreatic overgrowths on speleothems (POS) in Mallorca (Polyak et al., 2018) indicate a LIG highstand at 2.15 ± 0.75 m above present levels between ca. 126 and 116 ka (Fig. 8), which is ~5000 yr younger than our estimate. In this area, higher marine deposits were found at ca. 11 m a.s.l. (Hearty, 1987). However their LIG attribution is controversial. In fact, the age of deposits is not supported by chronological constrains and their formation can be related with older interglacial periods (e.g. MIS 11, Lorscheid et al., 2017). It is clear that there are open questions regarding the evidence from Mallorca and elsewhere in the

Mediterranean (e.g., Marra et al., 2019), which need to be addressed in the future.

6. Conclusion

Morpho-stratigraphic and geochronological investigations at Infreschi Cave allow us to precisely constrain the RSL highstand during MIS 5e at 8.90 ± 0.6 m a.s.l. as well as the timing of the end of highstand, with an estimated RSL drop of at least 6 m prior to 120 ka. This is consistent with some global mean sea-level curves indicating an early end of the MIS 5e highstand (Fig. 8), but in disagreement with the other scenarios of a late MIS 5e highstand. The model simulations based on the ICE-5G and ICE-6G scenarios are consistent with our data. However, further volumetric reduction of GrIS and AIS melting is required to reproduce the maximum of the observed RSL highstand, implying that GrIS and AIS retreat occurred early in MIS 5e. According to our chronology, there is no evidence of a secondary RSL highstand above 0 m a.s.l. following MIS 5e including during MIS 5a and MIS 5c.

Our results highlight the necessity for improving the chronology of Mediterranean sites, which can give important insights on sea-level evolution through the LIG and also on the behavior of present ice sheets, complementing far field data.

Credit author contribution

MB, GZ, FM, and LS conceived the research. MB, GZ, FM, LS and BG performed the fieldwork. JH and RD permed sample preparation and U/Th. GZ, BG, LM and MB performed the tephrostratigraphic investigations. PS performed model analyses. MB, GZ and BG prepared the first draft of the manuscript. All the authors contributed to the scientific discussion and final manuscript preparation.

Declaration of competing interest

The authors declare that they have no known competing financial interests or personal relationships that could have appeared to influence the work reported in this paper.

Acknowledgements

We thank Parco del Cilento, Valle di Diano e Alburni. This project has been partially funded by Fondi di Ateneo (to MB and GZ) and is an integration of the targets of the PRIN 2017 “FUTURE Project” (MIUR grant n. 20177TKBXZ_003, Leader GZ). We thank the students of the summer school held in 2018 in Marina di Camerota for their support during the field work.

Appendix A. Supplementary data

Supplementary data to this article can be found online at https://doi.org/10.1016/j.quascirev.2020.106658.

References

Ascione, A., Romano, P., 1999. Vertical movements on the eastern margin of the Tyrrhenian extensional basin. New data from Mt. Bulgheria (Southern Apennines, Italy). Tectonophysics 315, 337–356.

Asioli, A., Capotondi, L., Sironi, M.B.C., 2005. The Tyrrhenian stage in the Mediterranean: definition, usage and recognition in the deep-sea record. A proposal. Rendiconti dei Lincei 16, 297–310.

Aliyev, S.A., Saria, A., 2003. Biogenic accumulation of Uranium in recent seas. Acta Geol. Sin. 77, 372–381.

Ascione, A., Caiazzo, C., Hippolyte, J.C., Romano, P., 1997. Pliocene-Quaternary extensional tectonics and morphogenesis at the eastern margin of the southern tyrrhenian basin (Mt. Bulgheria, Campania, Italy). Il Quat. 10, 571–578.

Bard, E., Antonioli, F., Silenzi, S., 2002. Sea-level during the penultimate interglacial period based on submerged stalagmite from Argentarola Cave (Italy). Earth Planet Sci. Lett. 196 (3– 4), 135–146.

Bini, M., Isola, I., Zanchetta, G., Pappalardo, M., Ribolini, A., Ragaini, L., Baroni, C., Boretto, G., Fuck, E., Morigi, C., Salvatore, M.C., Bassi, D., Marzaioli, F., Terrasi, F., 2018. Middle holocene Relative Sea-level along atlantic patagonia: new data from camarones (chubut, Argentina). Holocene 28, 56–64.

Bonifay, E., Mars, P., 1959. Le Tyrrhénien dans le cadre de la chronologie quaternaire méditeranéenne. Bull. Soc. Geol. Fr. 7, 62–78.

Bourne, A.J., Albert, P.G., Matthews, I.P., Trincardi, F., Wulf, S., Asioli, A., Blockley, S.P.E., Keller, J., Lowe, J.J., 2015. Tephrochronology of core PRAD 1-2 from the Adriatic Sea: insights into Italian explosive volcanism for the period 200-80 ka. Quat. Sci. Rev. 116, 28–43.

Bourne, A.J., Lowe, J.J., Trincardi, F., Asioli, A., Blockley, S.P.E., Wulf, S., Matthews, I.P., Piva, A., Vigliotti, L., 2010. Distal tephra record for the last ca 105,000 years from core PRAD 1-2 in the central Adriatic Sea implications for marine tephrostratigraphy. Quat. Sci. Rev. 29, 3079–3094.

Chen, J.H., Curran, H.A., White, B., Wasserburg, G.J., 1991. Precise chronology ofthe last interglacial period: $^{234}U/^{230}Th$ data from fossil coral reefs in the Bahamas. Geol. Soc. Am. Bull. 103, 82–97.

Clark, P.U., Shakun, J.D., Marcott, S.A., Mix, A.C., Eby, M., Kulp, S., Levermann, A., Milne, G.A., Pfister, P.L., Santer, B.D., Schrag, D.P., Solomon, S., Stocker, T.F., Strauss, B.H., Weaver, A.J., Winkelmann, R., Archer, D., Bard, E., Goldner, A., Lambeck, K., Pierrehumbert, R.T., Plattner, G.K., 2016. Consequences of twenty-first-century policy for multi-millennial climate and sea-level change. Ch- Nature Climate Change, Nat- Climat 6, 360–369.

Colleoni, F., Wekerle, C., Naslund, J.-O., Brandefelt, J., Masina, S., 2016. Constraint on the penultimate glacial maximum Northern Hemisphere ice topography (~ 140 kyrs BP). Quat. Sci. Rev. 137, 97–112.

Creveling, J.R., Mitrovica, J.X., Hay, C.C., Austerm, J., Kopp, R.E., 2015. Revisiting tectonic corrections applied to Pleistocene sea-level Highstands. Quat. Sci. Rev. 111, 72–80.

DeConto, R.M., Pollard, D., 2016. Contribution of Antarctica to past and future sea-level rise. Nature 531, 591–597.

Dendy, S., Austermann, J., Creveling, J.R., Mitrovica, J.X., 2017. Sensitivity of Last Interglacial sea-level high stands to ice sheet configuration during Marine Isotope Stage 6. Quat. Sci. Rev. 171, 234–244.

Dutton, A., Lambeck, K., 2012. Ice volume and sea level during the last interglacial. Science 337, 216–219.

Dutton, A., Carlson, A.E., Long, A.J., Milne, G.A., Clarck, P.U., De Conto, R., Horton, B.P., Rahmstorf, S., Raymo, R.E., 2015. Sea-level rise due to polar ice-sheet mass loss during past warm periods. Science 349 (6244), aaa4019.

Esposito, C., Filocamo, F., Marciano, R., Romano, P., Santangelo, N., Santo, A., 2001. Genesi, evoluzione e paleogeografia delle grotte costiere di Marina di Camerota (Parco Nazionale del Cilento e Vallo di Diano, Italia Meridionale). Thalass. Salentina 26, 165–174.

Esposito, C., Filocamo, F., Marciano, R., Romano, P., Santangelo, N., Scarciglia, F., Tuccimei, P., 2003. Late-Quaternary shorelines in southern Cilento (Mt. Bulgheria): moprhostratigraphy and chronology. Il Quat. 16, 3–14.

Facenna, C., Becker, T.W., Aurer, K., Billi, A., Boschi, L., Brun, J.P., Capitanio, F.A., Funiciello, F., Horvàth, F., Jolivet, K., Piromallo, C., Royden, K., Rossetti, F., Serpelloni, E., 2013. Mantle dynamics in the mediterranean. Rev. Geophys. 52, 283–332. https://doi.org/10.1002/2013RG000444.

Farrell, W.E., Clark, J.A., 1976. On postglacial sea level. Geophys. J. Int. 46, 647–667.

Ferranti, L., Antonioli, F., Mauz, B., Amorosi, A., Dai Pra, G., Mastronuzzi, G., Monaco, C., Orrù, P., Pappalardo, M., Radke, U., Renda, P., Romano, P., Sansò, P., Verrubbi, V., 2006. Markers of the last interglacial sea-level high stand along the coast of Italy: tectonic implications. Quat. Int. 145–146, 30–54.

Fischer, H., Meissner, K.J., Mix, A.C., Abram, N.J., Austermann, J., Brovkin, V., Capron, E., Colombaroli, D., Daniau, A.L., Dyez, K.A., Felis, T., Finkelstein, S.A., Jaccard, S.L., McClymont, D.L., Rovere, A., Sutter, J., Wolff, E.W., Affolter, S., Bakker, P., Ballesteros-Cánovas, J.A., Barbante, C., Caley, T., Carlson, A.E., Churakova, O., Cortese, G., Brian, F., Cumming, B.F., Davis, B.A.S., de Vernal, A., Emile-Geay, J., Fritz, S.C., Gierz, P., Gottschalk, J., Holloway, M.D., Joos, F., Kucera, M., Loutre, M.-F., Daniel, J., Lunt, D.J., Marcisz, K., Marlon, J.R., Martinez, P., Masson-Delmotte, V., Nehrbass-Ahles, C., Otto-Bliesner, B.L., Raible, C.C., Risebrobak, B., Sánchez Goñi, M.F., Arrigo, J.S., Sarnthein, M., Sjolte, J., Stocker, T.F., Alvárez, P.A.V., Tinner, W., Valdes, P.J., Vogel, H., Wanner, H., Yan, Q., Yu, Z., Ziegler, M. Zhou L., 2018. Palaeoclimate constraints on the impact of 2 °C anthropogenic warming and beyond. Nature Geoscience, Nature Geosci 11, 474–485. https://doi.org/10.1038/s41561-018-0146-0.

Giaccio, B., Nomade, S., Wulf, S., Isaia, R., Sottili, G., Cavuoto, G., Galli, P., Messina, P., Sposato, A., Sulpizio, R., Zanchetta, G., 2012. The late MIS 5 Mediterranean tephra markers: a reappraisal from peninsular Italy terrestrial records. Quat. Sci. Rev. 56, 31–45.

Giaccio, B., Niespolo, E.M., Pereira, A., Nomade, S., Renne, P.R., Albert, P.G., Arienzo, I., Regattieri, E., Wagner, B., Zanchetta, G., Gaeta, M., Galli, P., Mannella, G., Peronace, E., Sottili, G., Florindo, F., Leicher, N., Marra, F., Tomlinson, E.T., 2017. First integrated tephrochronological record for the last ~190 kyr from the Fucino Quaternary lacustrine succession, central Italy. Quat. Sci. Rev. 158, 211–234.

Giaccio, B., Leicher, N., Mannella, G., Monaco, L., Regattieri, E., Wagner, B., Zanchetta, G., Gaeta, M., Marra, F., Nomade, S., Palladino, D.M., Pereira, A., Scheidt, S., Sottili, G., Wonik, T., Wulf, S., Zeeden, C., Ariztegui, D., Cavinato, G.P., Dean, J.R., Florindo, F., Leng, M.J., Macri, P., Niespolo, E., Renne, P.R., Christian, R., Sadori, L., Thomas, C., Tzedakis, P.C., 2019. Extending the tephra and palaeoenvironmental record of the Central Mediterranean back to 430 ka: a new core

from Fucino Basin, central Italy. Quat. Sci. Rev. https://doi.org/10.1016/j.quascirev.2019.106003.
Grant, K.M., Rohling, E.J., Bronk Ramsey, C., Cheng, H., Edwards, R.L., Florindo, F., Heslop, D., Marra, F., Roberts, A.P., Tamisiea, M.E., Williams, F., 2014. Sea-level variability over five glacial cycles. Nat. Commun. 5, 5076.
Hellstrom, J.C., 2003. Rapid and accurate U-Th dating using parallel ion counting multi-collector ICP-MS. J. Anal. Atomic Spectrom. 18, 135–136.
Hellstrom, J.C., 2006. U–Th dating of speleothems with high initial ^{230}Th using stratigraphical constraint. Quat. Geochronol. 1, 289–295.
Hearty, P.J., 1987. New data on the Pleistocene of Mallorca. Quat. Sci. Rev. 6 (3–4), 245–257.
Hearty, P.J., Miller, G.H., Stearns, C., Szabo, B.J., 1986. Aminostratigraphy of Quaternary shorelines around the Mediterranean basin. Geol. Soc. Am. Bull. 97, 850–858.
Hibbert, F.D., Rohling, E.J., Dutton, A., Williams, F.H., Chutcharavan, P.M., Zhao, C., Tamisiea, M.E., 2016. Coral indicators of past sea-level change: a global repository of U-series dated benchmarks. Quat. Sc.Rev. 145, 1–56.
Higham, T., Douka, K., Wood, R., Ramsey, C.B., Brock, F., Basell, L., Camps, M., Arrizabalaga, A., Baena, J., Barroso-Ruíz, C., Bergman, C., Boitard, C., Boscato, P., Caparros, M., Conard, N.J., Draily, C., Froment, A., Galvan, B., Gambassini, P., Garcia-Moreno, A., Grimaldi, S., Haesaerts, P., Holt, B., Iriarte-Chiapusso, M.-J., Jelinek, A., Jord_a Pardo, J.F., Maíllo-Fern_andez, J.-M., Marom, A., Maroto, J., Menendez, M., Metz, L., Morin, E., Moroni, A., Negrino, F., Panagopoulou, E., Peresani, M., Pirson, S., De La Rasilla, M., Riel-Salvatore, J., Ronchitelli, A., Santamaria, D., Semal, P., Slimak, L., Soler, J., Soler, N., Villaluenga, A., Pinhasi, R., Jacobi, R., 2014. The timing and spatiotemporal patterning of Neanderthal disappearance. Nature 512, 306–309.
Hillaire-Marcel, C., Gariépy, C., Ghaleb, B., Goy, J.L., Zazo, C., Barcelo, J.C., 1996. U-series measurements in Tyrrhenian deposits from mallorca - further evidence for two last-interglacial high sea levels in the Balearic Islands. Quat. Sci. Rev. 15 (1), 53–62.
Insinga, D.D., Tamburrino, S., Lirer, F., Vezzoli, L., Barra, M., De Lange, G.J., Tiepolo, M., Vallefuoco, M., Mazzola, S., Sprovieri, M., 2014. Tephrochronology of the astronomically-tuned KC01B deep-sea core, Ionian Sea: insights into the explosive activity of the Central Mediterranean area during the last 200 ka. Quat. Sci. Rev. 85, 63–84.
Iorio, M., Liddicoat, J., Budillon, F., et al., 2014. Combined palaeomagnetic secular variation and petrophysical records to time constrain geological and hazardous events: an example from the eastern Tyrrhenian Sea over the last 120 ka. Gl. Planet. Ch, 113, 91–109.
Issel, A., 1914. Lembi fossilferi quaternari e recenti nella Sardegna meridionale. Accad. Naz. Lincei (Fondazione Leone Caetani) 5, 759–770.
Ivanovich, M., Vita-Finzi, C., Henning, G.J., 1983. Uranium-series dating of molluscs from uplifted Holocene beaches in the Persian Gulf. Nature 302, 408–410.
Jedoui, Y., Reyss, L., Kallel, N., Montacer, M., BenIsmayl, H., Davaud, E., 2003. U-series evidence for two high Last Interglacial sea levels in southeastern Tunisia. Quat. Sci. Rev. 22, 343–351.
Kaspar, F., Kühl, N., Cubasch, U., Litt, T., 2005. A model-data comparison of European temperatures in the Eemian interglacial. Geophys. Res. Lett. 32, L11703. https://doi.org/10.1029/2005GL022456.
Khan, N.S., Horton, B.P., Engelhart, S., Rovere, A., Vacchi, M., Ashe, E.L., Shennan, I., 2019. Inception of a global atlas of sea levels since the Last Glacial Maximum. Quat. Sci. Rev. 220, 359–371.
Kopp, R.E., Simons, F.J., Mitrovica, J.X., Maloof, A.C., Oppenheimer, M., 2009. Probabilistic assessment of sea level during the last interglacial stage. Nature 462, 863–867.
Laborel, J., Laborel-Deguen, F., 1996. Biological indicators of Holocene sea-level and climatic variations on rocky coasts of tropical and subtropical regions. Quat. Int. 31, 53–60.
Lambeck, K., Purcell, A., Funder, S., Kjaer, K.H., Larsen, E., Moller, P., 2006. Constraints on the Late Saalian to early Middle Weichselian ice sheet of Eurasia from field data and rebound modelling. Boreas. https://doi.org/10.1080/03009480600781875.
Le Bas, M.J., Le Maitre, R.W., Streckeisen, A., Zanettin, B., 1986. A chemical classification of volcanic rocks based on the total alkali-silica diagram. J. Petrol. 27, 745–750.
Leicher, N., Zanchetta, G., Sulpizio, R., Giaccio, B., Wagner, B., Nomade, S., Francke, A., Del Carlo, P., 2016. First tephrostratigraphic results of the DEEP site record from Lake Ohrid (Macedonia and Albania). Biogesciences 13, 2151–2178.
Lisiecki, L.E., Raymo, M.E., 2005. A Pliocene-Pleistocene stack of 57 globally distributed benthic δ^{18}O records. Paleoceanography 20, PA1003. https://doi.org/10.1029/2004PA001071.
Lorscheid, T., Stocchi, P., Casella, E., Gómez-Pujol, L., Vacchi, M., Mann, T., Rovere, A., 2017. Paleo sea-level changes and relative sea-level indicators: precise measurements, indicative meaning and glacial isostatic adjustment perspectives from Mallorca (Western Mediterranean). Palaeogeogr. Palaeoclimatol. Palaeoecol. 473, 94–107.
Mannella, G., Giaccio, B., Zanchetta, G., Regattieri, E., Niespolo, E.M., Pereira, A., Renne, P.R., Nomade, S., Leicher, N., Perchiazzi, N., Wagner, B., 2019. Palaeoenvironmental and palaeohydrological variability of mountain areas in the central Mediterranean region: a 190 ka-long chronicle from the independently dated Fucino palaeolake record (central Italy). Quat. Sci. Rev. 210, 190–210.
Marino, G., Rohling, E.J., Rodrìguez-Sanz, L., Grant, K.M., Heslop, D., Roberts, A.P., Stanford, J.D., Yu, J., 2015. Bipolar seesaw control on last interglacial sea level. Nature 197, 197–201.
Martini, F., 2015. Cilento le Origini. Preistoria, arte e vita dei popoli cacciatori-raccoglitori. Museo e Istituto Fiorentino di Preistorioa, Firenze, p. 134.
Marra, F., Bahain, J.-J., Jicha, B.R., Nomade, S., Palladino, D.M., Pereira, A., Tolomei, C., Pierre Voinchet, P., Anzidei, M., Aureli, D., Ceruleo, P., Falguères, C., Florindo, F., Gatta, M., Ghaleb, B., La Rosa, M., Peretto, C., Petronio, C., Rocca, R., Rolfo, M.F., Salari, L., Smedile, A., Tombret, O., 2019. Reconstruction of the MIS 5.5, 5.3 and 5.1 coastal terraces in Latium (central Italy): a re-evaluation of the sea-level history in the Mediterranean Seaduring the last. Quat. Int. 525, 54–77.
Mauz, B., 1999. Late Pleistocene records of littoral processes at the Tyrrhenian Coast (Central Italy): depositional environments and luminiscence chronology. Quat. Sci. Rev. 18, 1173–1184.
McKay, N.P., Overpeck, J.T., Otto-Bliesner, B.L., 2011. The role of ocean thermal expansion in Last Interglacial sea level rise. Geophys. Res. Lett. 38, L14605. https://doi.org/10.1029/2011GL048280.
Medina-Elizalde, M., 2013. A globalcompilationofcoralsea-levelbenchmarks:Implicationsand new challenges. Earth Planet Sci. Lett. 362, 310–318.
Miller, L., Douglas, B.C., 2004. Mass and volume contributions to twentieth-century global sea level rise. Nature 428, 406–409.
Mitrovica, J.X., Davis, J.L., Shapiro, I.I., 1994. A spectral formalism for computing three-dimensional deformations due to surface loads. J.Geoph. Res. 99, 7057–7073.
Moseley, G.E., Smart, P.L., Richards, D.A., Hoffmann, D.L., 2013. Speleothem constraints on marine isotope stage (MIS) 5 relative sea levels, Yucatan Peninsula, Mexico. J. Quat. Sci. 28, 293–300.
Muhs, D.R., Simmons, K.R., Meco, J., Porat, N., 2015. Uranium-series ages of fossil corals from Mallorca, Spain: the “Neotyrrhenian” high stand of the Mediterranean Sea revisited. Palaeogeogr. Palaeoclimatol. Palaeoecol. 438, 408–424.
O'Leary, M.J., Hearty, P.J., Thompson, W.G., Raymo, M.E., Mitrovica, J.X., Webster, J.M., 2013. Ice sheet collapse following a prolonged period of stable sea level during the last interglacial. Nat. Geosci. 6, 796–800.
Otto-Bliesner, B.-L., Rosenbloom, N., Stone, E.J.-, McKay, N.P., Lunt, D.J., Brady, E.C., Overpeck, J.T., 2013. How warm was the last interglacial? New model-data comparisons. Philos. Trans. R. Soc. London, Ser. A 371, 20130097. https://doi.org/10.1098/rsta.2013.0097.
Padgett, J.S., Engelhart, S.E., Hoffmann, G., Rosentau, A., Yu, F., 2018. Sea-level change from minutes to millennia: first meeting of IGCP Project 639 in Oman. Episodes 41, 115–118.
Peltier, W.R., 2004. Global glacial isostasy and the surface of the ice-age Earth: the ICE-5G (VM2) model and GRACE. Annu. Rev. Earth Planet Sci. 32, 111–149.
Peltier, W.R., Argus, D.F., Drummond, R., 2015. Space geodesy constrains ice-age terminal deglaciation: the global ICE-6G_C (VM5a) model. J. Geophys. Res. Solid Earth 120, 450–487. https://doi.org/10.1002/2014JB011176.
Pérès, J.M., Picard, J., 1964. Nouveau Manuel de Bionomie Benthique de la Mer Mediterranée. Recueil des Travaux de la Station Marine d'Endoume. Bull. (Arch. Am. Art) 31 (47), 5–137.
Polyak, V.J., Onac, B.P., Fornós, J.J., Hay, C., Asmerom, Y., Dorale, J.A., Ginés, J., Tuccimei, P., Ginés, A., 2018. A highly resolved record of relative sea level in the western Mediterranean Sea during the last interglacial period. Nat. Geosci. 11, 860–864.
Railsback, L.B., Gibbard, P.L., Head, M.J., Voarintsoa, N.R.G., Toucanne, S., 2015. An optimized scheme of lettered marine isotope substages for the last 1.0 million years, and the climatostratigraphic nature of isotope stages and substages. Quat. Sci. Rev. 111, 94–106.
Regattieri, E., Giaccio, B., Zanchetta, G., Drysdale, R.N., Galli, P., Nomade, S., Peronace, E., Wulf, S., 2015. Hydrological variability over Apennine during the Early Last Glacial precession minimum, as revealed by a stable isotope record from Sulmona basin, central Italy. J. Quat. Sci. 30, 19–31.
Rohling, E.J., Hibbert, F.D., Williams, F.H., Grant, K.M., Marino, G., Foster, G.L., Hennekam, R., de Lange, G.J., Roberts, A.P., Yu, J., Webster, J.M., Yokoyama, Y., 2017. Differences between the last two glacial maxima and implications for ice-sheet, δ^{18}O, and sea-level reconstructions. Quat. Sci. Rev. 176, 1–28.
Rohling, E.J., Hibbert, F.D., Grant, K.M., Galaasen, E.V., Irvali, N., Kleiven, H.F., Marino, G., Ninnemann, U., Roberts, A.P., Rosenthal, Y., 2019. Asynchronous Antarctic and Greenland ice-volume contributions to the last interglacial sea-level highstand. Nat. Commun. 10, 5040. https://doi.org/10.1038/s41467-019-12874-3.
Rovere, A., Antonioli, F., Bianchi, C.N., 2015. Chapter 18. Fixed biological indicators. In: Shennan, A., Horton, B.P. (Eds.), Handbook of Sea-Level Research. Pag. 268-280. Wiley & Sons Ltd.
Rovere, A., Raymo, M.E., Vacchi, M., Lorscheid, T., Stocchi, P., Gómez-Pujol, L., Harris, D.L., Casella, E., O'Leary, M.J., Hearty, P.J., 2016. The analysis of Last Interglacial (MIS 5e) relative sea-level indicators: reconstructing sea-level in a warmer world. Earth Sci. Rev. 159, 404–427.
Sarti, L., 1996. Porto Infreschi (S. Giovanni a Pito, Salerno). Preistoria e Protostoria. Guide archeologiche. XIII Congr. Int. U.I.S.P.P, 1996 Forlì 43–49.
Siddall, M., Rohling, E.J., Almogi-Labin, A., Hemleben, Ch, Meischner, D., Schmelzer, I., Smeed, D.A., 2003. Sea-level fluctuations during the last glacial cycle. Nature 423, 853–858.
Schembri, P.J., Deidun, A., Mallia, A., Marcieca, L., 2005. Rocky shore biotic assemblages of the Maltese Islands (Central Mediterranean): a conservation perspective. J. Coast Res. 21, 157–166.
Shennan, I., Long, A., Horton, B.P., 2015. Handbook of Sea-Level Research. John Wiley & Sons. Ltd.
Stirling, C.H., Esat, T.M., Lambeck, K., McCulloch, M.T., 1998. Timing and duration of the last interglacial; evidence for a restricted interval of widespread coral reef

growth. Earth Planet Sci. Lett. 160, 745–762.
Stocchi, P., Spada, G., 2007. Glacio and hydro-isostasy in the Mediterranean Sea: clark's zones and role of remote ice sheets. Ann. Geophys. 50, 741–761.
h Stocchi, P., Vacchi, V., Lorscheid, T., de Boer, B., Simms, A.R., van de Wal, R.S.W., Vermeersen, B.L.A., Pappalardo, P., Rovere, A., 2018. MIS 5e relative sea-level changes in the Mediterranean Sea: contribution of isostatic disequilibrium. Quat.Sc. Rev. 185, 122–134.
Sulpizio, R., Zanchetta, G., D'Orazio, M., Vogel, H., Wagner, B., 2010. Tephrostratigraphy and tephrochronology of lakes Ohrid and prespa, balkans. Biogeosciences 7, 3273–3288.
Tomlinson, E.L., Arienzo, I., Civetta, L., Wulf, S., Smith, V.C., Hardiman, M.S., Lane, C.S., Carandente, A., Orsi, G., Rosi, M., Muller, W., Menzies, M.A., 2012. Geochemistry of the Phlegraean Fields (Italy) proximal sources for major Mediterranean tephras: implications for the dispersal of Plinian and coignimbritic components of explosive eruptions. Geochem. Cosmochim. Acta 93, 102–128.
Tomlinson, E.L., Smith, V.C., Albert, P.G., Aydar, E., Civetta, L., Cioni, R., Çubukçu, E., Gertisser, R., Isaia, R., Menzies, M.A., Orsi, G., Rosi, M., Zanchetta, G., 2015. The major and trace element glass compositions of the productive Mediterranean volcanic sources: tools for correlating distal tephra layers in and around Europe. Quat. Sci. Rev. 118, 48–66.
Vacchi, M., Ermolli, E.R., Morhange, C., Ruello, M.R., Di Donato, V., Di Vito, M.A., Boetto, G., 2020. Millennial variability of rates of sea-level rise in the ancient harbour of Naples (Italy, western Mediterranean Sea). Quat. Res. 93, 284–298.
van de Plassche, O., 1986. Sea-level Research: A Manual for the Collection and Evaluationof Data. Geobooks, Norwich, p. 618.
Vesica, P.L., Tuccimei, P., Turi, B., Fornós, J.J., Ginés, A., Ginés, J., 2000. Late Pleistocene Paleoclimates and sea-level change in the Mediterranean as inferred from stable isotope and U-series studies of overgrowths on speleothems, Mallorca, Spain. Quat. Sci. Rev. 200, 865–879.
Waelbroeck, L., Labeyrie, E., Duplessya, J.C., McManusc, J.F., Lambeck, K., Balbona, E., Labracherie, M., 2002. Sea-level and deep water temperature changes derived from benthic foraminifera isotopic records C. Quat. Sci. Rev. 21, 295–305.
Wulf, S., Keller, J., Paterne, M., Mingram, J., Lauterbach, S., Opitz, S., Sottili, G., Giaccio, B., Albert, P.G., Satow, C., Tomlinson, E.L., Viccaro, M., Brauer, A., 2012. The 100-133 ka record of Italian explosive volcanism and revised tephrochronology of Lago Grande di Monticchio. Quat. Sci. Rev. 58, 104–123.
Wulf, S., Hardiman, M.J., Staff, R.A., Koutsodendris, A., Appelt, O., Blockley, S.P.E., Lowe, J.J., Manning, C.J., Ottolini, L., Schmitt, A.K., Smith, V.C., Tomlinson, E.L., Vakhrameeva, P., Knipping, M., Kotthoff, U., Milner, A.M., Müller, U.C., Christanis, K., Kalaitzidis, S., Tzedakis, C.P., Schmiedl, G., Pross, J., 2018. The marine isotope stage 5 cryptotephra record of Tenaghi Philippon, Greece: towards a detailed tephrostratigraphic framework for the Eastern Mediterranean region. Quat. Sci. Rev. 186, 236–262.
Zanchetta, G., Bonadonna, F.P., Marcolini, F., Ciampalini, A., Fallick, A.E., Leone, G., Michelucci, L., 2004. Intra-Tyrrhenian cooling event deduced by non-marine mollusc assemblage at Villa S. Giorgio (Livorno, Italy). Boll. Soc. Paleontol. It. 43, 331–343.
Zanchetta, G., Bini, M., Isola, I., Pappalardo, M., Ribolini, A., Consoloni, I., Boretto, G., Fucks, E., Ragaini, L., Terrasi, F., 2014. Middle-to late-Holocene relative sea-level changes at Puerto Deseado (Patagonia, Argentina). Holocene 24, 307–317.
Zanchetta, G., Giaccio, B., Bini, M., Sarti, L., 2018. Tephrostratigraphy of Grotta del Cavallo, Southern Italy: insights on the chronology of Middle to Upper Palaeolithic transition in the Mediterranean. Quat. Sci. Rev. 182, 65–77.
Zanchetta, G., Regattieri, E., Giaccio, B., Wagner, B., Sulpizio, R., Francke, A., Vogel, H., Sadori, L., Masi, A., Sinopoli, G., Lacey, J.H., Leng, M.J., Leicher, N., 2016. Aligning and synchronization of MIS5 proxy records from Lake Ohrid (FYROM) with independently dated Mediterranean archives: implications for DEEP core chronology. Biogeosciences 13, 2757–2768.